15th IFK
Proc. of the 15th International Fluid Power Conference <Symposium/Conference>
<DOI>

Automated Steering Control for Articulated Off-Highway Machines

Zezhou Wang[1]*, Magdalena Janocha[1], Lukas Michiels, Benjamin Kazenwadel[1], Marcus Geimer[1]

[1]*Institute of Mobile Machines, Karlsruhe Institute of Technology*

** Corresponding author: Zezhou Wang (zezhou.wang@kit.edu)*

Abstract.

Automated steering control is a more and more important function for Articulated Off-Highway Machines (AOHMs) operating in construction, mining, and forestry. Their articulation-based kinematics enable high maneuverability but also introduce challenges for lateral control, particularly when tracking paths with large curvature or frequent directional changes. In the forestry industry, AOHMs must achieve precise and stable path tracking in unstructured environments, where disturbances and dynamic path updates are common. This paper investigates a combined control approach that combines a Pure Pursuit (PP) and a Stanley (ST) controller into a feedforward–feedback framework tailored to AOHMs. As an example application in an AOHM, a forwarder is used in simulations on four representative paths—circular, sinusoidal, straight, and real-world trajectories—in both forward and backward driving. The results show that the PP-ST controller consistently outperforms the individual controllers, achieving maximum lateral errors below 0.2 m across all test paths. Robustness analysis under dynamic steering and velocity noise, payload variation, and initial offsets demonstrates convergence in all cases, with steady-state lateral errors remaining within 0.1 m. Even for extreme orientation deviations at the initial position, the controller eventually corrects the trajectory and returns to the reference path. Overall, the PP–ST controller provides accurate, stable, and robust lateral control for articulated off-highway machines in representative forestry scenarios.

Keywords. Assistance systems, articulated vehicle, lateral control, mobile machine, Pure Pursuit, Stanley.

1. INTRODUCTION

Nowadays, off-highway mobile working machines play a critical role in industries such as construction, mining, and forestry, where operations are performed in unstructured and often challenging environments [1]. Automated driving technology for these machines has the potential to enhance safety, reduce operator fatigue, and improve overall productivity [2]. By enabling precise navigation and efficient task execution, these systems can also help optimize fuel usage and minimize environmental impact [3].

Within this category, Articulated Off-Highway Machines (AOHMs)—comprising multiple rigid units connected via articulation joints—are widely adopted due to their exceptional maneuverability in confined spaces [4]. The articulated steering mechanism enables tight turning radii and improved mobility on complex terrain. However, the kinematic complexity introduced by articulation makes lateral control more challenging than for rigid-frame vehicles, requiring control strategies capable of handling large steering angles and rapid changes in path curvature.

AOHMs are frequently deployed in the forestry industry, in machines like forwarders and harvesters, where precise lateral control is essential for safe and efficient operation. Reliable environmental perception—such as detecting and parameterizing individual trees—is a prerequisite for navigating the narrow and irregular lanes found in forest environments, often on uneven and unstructured terrain [5]. In such conditions, the planned path is continuously updated in response to changes in the surrounding environment and operational demands. Consequently, the lateral control system must not only achieve high tracking accuracy on paths with large curvature and frequent directional changes but also adapt in real time to sudden adjustments while maintaining vehicle stability.

In addition to the single-joint configuration that dominates current forestry machines, multi-articulated vehicle architectures have been investigated in the broader field of heavy-duty vehicle dynamics and control. Examples include multi-unit articulated systems comprising dual multi-axle trailers with coordinated steering for motion control [6]. Further studies have analyzed articulated multi-body vehicle systems that combine articulated joints and other joint types to capture complex interactions between interconnected units [7]. This paper focuses on AOHMs with a single articulation joint between the front and rear units, which remains the prevailing design in forestry applications such as forwarders and harvesters.

Among the existing lateral control methods, geometric approaches such as the Pure Pursuit (PP) and Stanley (ST) controllers are well known for their robustness, simplicity, and suitability for real-time implementation [8]. This work adapts and integrates these two controllers into a feedforward–feedback framework tailored to the kinematics of articulated off-highway machines, aiming to achieve robust and precise path tracking under diverse and dynamic operating conditions, including those encountered in forestry operations.

2. Lateral Control Methods for All-Wheel-Driven Articulated Off-Highway Machines

In this section, the kinematics of AOHMs are described, followed by the introduction of two lateral control methods: The Pure Pursuit and the Stanley controller.

Advanced control approaches such as Model Predictive Control (MPC) and nonlinear MPC require accurate dynamic vehicle models, reliable state estimation and considerable real-time computational resources. For articulated vehicles, tube-based robust MPC for tracking control explicitly relies on a detailed vehicle model and online optimization of the control sequence [9]. Nonlinear MPC for underground articulated vehicles is based on a high-fidelity dynamic model and nonlinear optimization at each control step [10], and multi-time-scale predictive control for underground articulated vehicles further illustrates the

computational effort associated with predictive control in this class of machines [11]. Robust path-following control for articulated heavy-duty vehicles addresses model uncertainty but still requires substantial tuning and validation effort to guarantee performance across the operating range [12]. In contrast, geometric controllers such as PP and ST controller operate with a kinematic model and low computational cost, which makes them suitable for real-time implementation on AOHMs. These characteristics motivate the use of the combined PP and ST controller in this work.

2.1. Kinematics of the Articulated Off-Highway Machine

Figure 2.1 illustrates the geometry of an AOHM. The steering angle δ can be derived from the orientation angles θ_i of the vehicle units [13]:

$$\delta = \theta_2 - \theta_1 \qquad (2.1)$$

A (virtual) axle can be defined between the two wheels of each vehicle unit. From the midpoint of this axle to the articulation joint, the lengths l_i and the corresponding radii r_i to a virtual center of rotation center o— about which the AOHM moves during a steering maneuver — can be determined. The radii are given by [13]:

$$r_1 = \frac{l_1 \cdot cos(\delta) + l_2}{sin(\delta)} \qquad (2.2)$$

$$r_2 = \frac{l_2 \cdot cos(\delta) + l_1}{sin(\delta)} \qquad (2.3)$$

To standardize the motion orientation of the AOHM, a quasi-static planar kinematic model is considered. When the machine moves forward, the pose reference point is defined at the front axle center; when moving backward, it is defined at the rear axle center. Under this kinematic assumption (negligible tire slip and compliance), r_1 and r_2 in Eq. (2.2) and Eq. (2.3) denote the instantaneous curvature radii of the chosen reference point. These radii are geometric quantities only and do not represent the actual turning radius, which in practice is influenced by payload, tire–soil interaction, velocity, and vehicle dynamics.

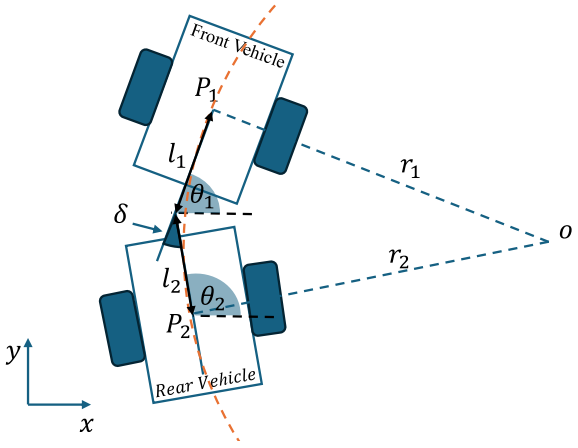

Figure 2.1. Geometry of an Articulated Off-Highway Machine

2.2. Pure Pursuit Controller for AOHM

The Pure Pursuit controller steers the vehicle toward a target point located at a specified lookahead distance l_d along the planned path [14, 15]. The lookahead distance is

$$l_d = max\left(l_{d,min}, min\left(k_{PP} \cdot |v|, l_{d,max}\right)\right) \quad (2.4)$$

where v is the current vehicle speed, k_{PP} is the speed gain, and $l_{d,min}$, $l_{d,max}$ are the allowable bounds. This distance is smoothed to prevent abrupt steering changes.

As illustrated in Figure 2.2, l_d is measured along the reference path from the vehicle's current projected position to the lookahead point. The angle α is the heading from the vehicle to the lookahead point, while $\Delta\psi_1$ and $\Delta\psi_2$ are orientation differences between the Pure Pursuit arc and the reference path at the first and second candidate lookahead points, respectively. An orientation difference check reduces l_d in highly curved segments until $|\Delta\psi|$ falls below a predefined threshold, improving stability in dynamic paths.

Once the lookahead point is determined, the turning radius R can be calculated [16]:

$$R = \frac{l_d}{2 \cdot sin\alpha} \quad (2.5)$$

By applying the tangent half-angle substitution, where $t = \tan\frac{\delta_{PP}}{2}$, and considering the forward motion case in which the turning radius $R = r_1$, Eq. (2.2) can be transformed into:

$$(l_1 - l_2) \cdot t^2 + 2\, r_1\, t - l_1 - l_2 = 0 \quad (2.6)$$

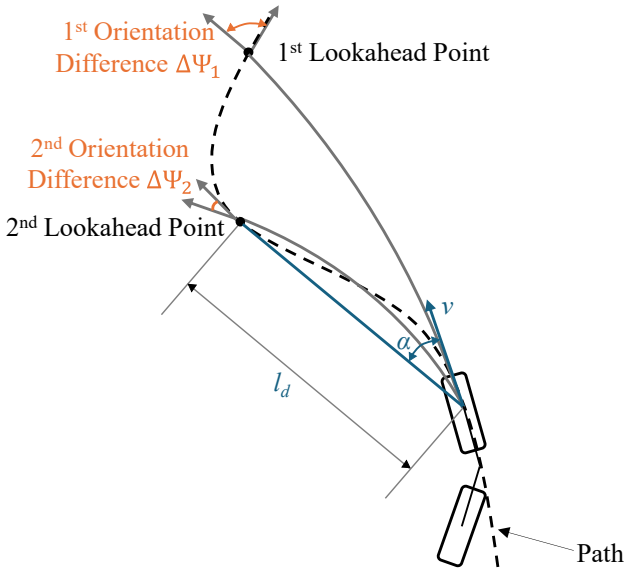

Figure 2.2. Selection of Lookahead Point for Pure Pursuit Controller

The steering angle of the Pure Pursuit controller for AOHM can then be obtained by applying the quadratic formula:

$$\delta_{PP} = 2\left(\tan^{-1}\left(\frac{-r_1 \pm \sqrt{l_1^2 - l_2^2 + r_1^2}}{l_1 - l_2}\right) + \pi n\right), \quad n \in Z \tag{2.7}$$

The same applies to the backward motion case, where r_1 in Eq. (2.6) and Eq. (2.7) is replaced by r_2 from Eq. (2.3), and n denotes the periodicity of the tangent function.

2.3. Stanley Controller for AOHM

The Stanley controller, similar to the Pure Pursuit controller, is employed for the lateral control of vehicles. However, instead of relying on a fixed lookahead point as in the Pure Pursuit controller, the Stanley controller determines the steering command based on the path point that is closest to the vehicle along its heading direction. To prevent oscillatory steering behavior when the reference point is too close, a lookahead distance is introduced in practice. Compared to the Pure Pursuit controller, the Stanley controller is generally more effective in suppressing lateral errors and achieving higher path-tracking accuracy, particularly in low-speed or sharp-turn scenarios [17].

The Stanley controller is a geometric method for lateral vehicle control that simultaneously corrects the heading error and the lateral position error to align the vehicle with the planned path. As shown in Figure 2.3, (c_x, c_y) denotes the closest point on the path to the AOHM's current reference point, e_l is the signed lateral error measured perpendicularly from this closest point to the vehicle reference point, and θ_h is the heading error between the longitudinal axis of AOHM's front vehicle and the tangent direction of the path at (c_x, c_y). The front vehicle's longitudinal speed at the reference point is denoted by v, and δ_{ST} is the steering command generated by the controller.

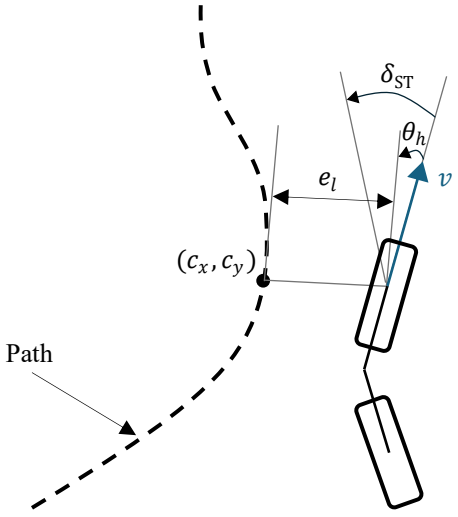

Figure 2.3. Stanley Controller for AOHM

In this work , based on the original Stanley controller, as proposed by Hoffmann et al. [18], a small positive constant k_v is integrated in the denominator to suppress excessive steering

at very low speeds and to avoid division by zero. The Stanley steering angle can be computed as

$$\delta_{ST} = \theta_h + \arctan\left(\frac{k_l e_l}{v + k_v}\right) \tag{2.8}$$

where the lateral correction term scales inversely with the vehicle's speed v, and k_l is the lateral error gain that scales the correction based on the magnitude of e_l. The first term in the equation corrects the heading to match the path's tangent direction, while the second term drives the lateral error toward zero. This combination allows the controller to achieve accurate path tracking across a wide range of speeds and curvature conditions.

3. Overall Framework of Automated Steering Control for Articulated Off-Highway Machines

The feasibility of combining the Pure Pursuit (PP) and Stanley (ST) controllers has been proved for robust lateral path tracking of indoor mobile robots [19]. Building upon this concept, the PP–ST combination will be adapted to the lateral control of AOHMs.

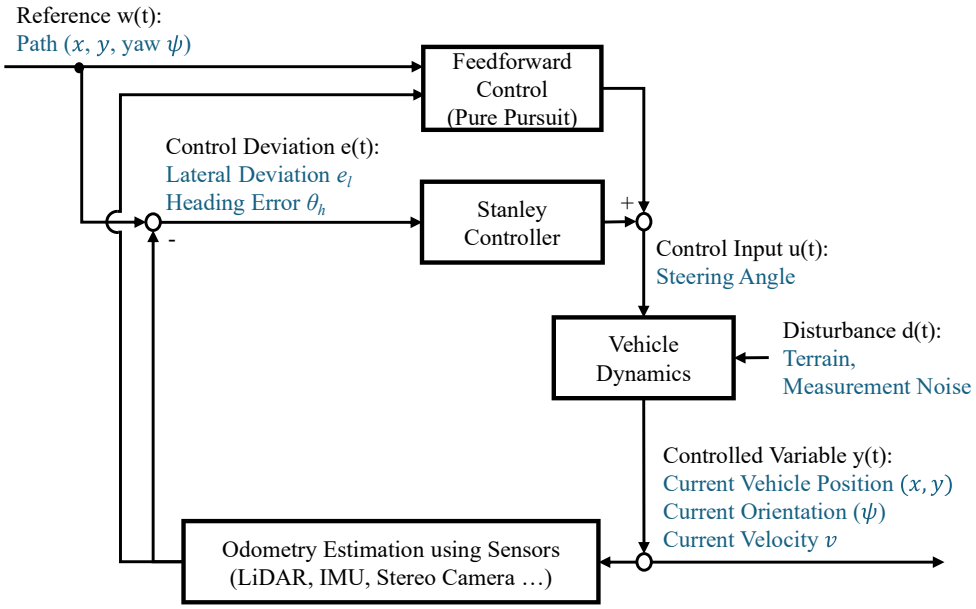

Figure 3.1. Overall Framework of Automated Steering Control for AOHMs

The overall framework is illustrated in Figure 3.1. In this framework, the planned path is available from a higher-level planning module, which generates a sequence of target poses (x, y, ψ) based on environmental perception and task objectives. At each control step, the vehicle's current pose and velocity are obtained from the odometry estimation module. A feedforward–feedback strategy is applied to generate the steering command: the PP module

determines the curvature required to reach a look-ahead point on the planned path, while the ST controller compensates for both lateral displacement and heading misalignment relative to the nearest path point. The outputs of both controllers are summed to form the steering angle command, which is sent to the articulated steering joint via the vehicle's actuation interface. The resulting vehicle motion is continuously monitored, closing the control loop and enabling precise path tracking under the kinematic constraints of articulated steering.

4. SIMULATION SETUPS

In this paper, a Forwarder is used as an exemplary application of the proposed control schematics.

Table 1: Technical Specifications of the Test Vehicle

Technical Specifications			
Total length (m)	10.96	Curb Weight (kg)	18,500
Width (m)	3.0	Maximum Payload (t)	14
Height (m)	3.79	Weight Distribution	60/40 (Front/Rear)
Front Axle Length l_1 (m)	1.799	Tire Diameter (m)	1.312
Rear Axle Length l_2 (m)	3.480	Tire Width (m)	1.42
Maximum Articulation Angle δ_{max} (°)	30	Ground Friction (rolling / static)	0.35 / 0.45

The Forwarder will be simulated in MATLAB Simulink with Simscape Multibody, where the forwarder is represented as a multi-body system including the articulated steering joint and axle constraints listed in Table 1. Tire–ground interaction is modeled with constant rolling and static friction coefficients (0.35 / 0.45). A variable-step solver with adaptive step sizes is applied to ensure numerical stability of multi-body dynamics. The simulation horizon is adjusted to allow traversal of each path. Outputs such as pose, steering angle, and lateral error are sampled at every time step.

In the simulations, the vehicle pose and velocity are provided as ideal ground-truth states from the multibody model without sensor noise. This assumption isolates the controller performance from perception uncertainties and allows a focused evaluation of the lateral control scheme. The initial forward velocity is set to a baseline value of 2 m/s, which corresponds to typical low-speed operation of forestry machinery and is used as the nominal input for all simulated scenarios.

The Forwarder will be tested on four paths: a circular path, a sinusoidal path, a straight line, and a real-world path collected from the Forwarder in the forest.

The formulas of the first three paths are defined in Table 2, where x starts from 0 m and path points are sampled every 0.5 m, resulting in a total of 150 points forming the final path. On each path, the Forwarder is tested once in forward and once in backward direction, i.e.,

evaluating the lateral control performance when either the front or the rear vehicle is leading. In addition, to investigate the robustness of the lateral controllers, further simulations are conducted on the sinusoidal path by introducing various disturbances, including dynamic steering and velocity noise, payload variations, and initial offsets.

Table 2: Equations of the Test Path

Path	Equation
Circular Path	$y_{circular}(x) = -12 \pm \sqrt{12^2 - x^2}$
Sinusoidal Path	$y_{sin}(x) = 5 \cdot \sin(x/10)$
Straight Line	$y_{straight}(x) = 0$

For the PP and ST controllers, the relevant parameters in Eq. (2.4) and Eq. (2.8) are listed in Table 3. These parameters are determined based on a sinusoidal path defined by $f_{\sin 2}(x) = 20 \cdot \sin(x/20)$, which will be detailed in subsequent sections.

Table 3: Parameters of Lateral Controllers

Parameter	Value
Maximum Lookahead Distance $l_{d,max}$ (m)	15.0
Minimum Lookahead Distance $l_{d,min}$ (m)	2.0
Speed Gain of PP controller k_{pp} (s)	3.0
Orientation Difference $\Delta\Psi$ (°)	20
Step Size for Orientation-Difference $\Delta\Psi$ Adaptation (m)	0.5
Velocity Offset k_v (m/s)	0.1
Lateral Error Gain k_l (s^{-1})	5.0

5. RESULTS AND ANALYSIS

In the following sections, simulations based on the setups described in Section 4 are conducted to evaluate the performance of the PP-ST controller introduced in Section 3. First, the optimal ST controller parameters, such as lateral error gain k_l, are determined through parameter variation. Next, the path-tracking performance of the PP-ST controller is compared with that of the standalone PP and ST controllers. Finally, different disturbance scenarios are introduced in the simulations to investigate the robustness of the PP-ST controller.

5.1. Parameter Tuning of the PP–ST Controller

In this paper, the controller parameters are tuned using a trial-and-error–based, simulation-driven approach. To illustrate the tuning procedure, the lateral error gain k_l of the ST controller is selected as a representative example.

As shown in Eq. (2.8), the lateral error gain k_l is a key parameter influencing the performance of the ST controller. The following simulations are conducted on the previously defined $f_{sin2}(x)$ path using different values of k_l to determine the optimal setting.

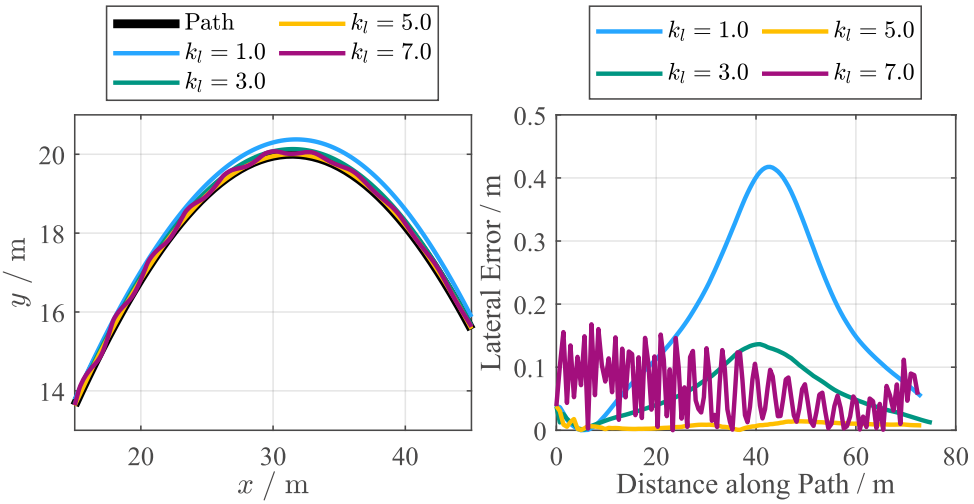

Figure 5.1. Optimization of Stanley Controller's Lateral Error Gain

As illustrated in Figure 5.1, four cases are compared: $k_l = 1.0$, $k_l = 3.0$, $k_l = 5.0$, and $k_l = 7.0$. The left-hand side of the figure presents the path-tracking results of the ST controller under different k_l values, while the right-hand side shows the corresponding lateral errors relative to the reference path. It can be observed that when $k_l = 1.0$, the lateral error is relatively large, particularly in sections with higher curvature. As k_l increases, for example to 3.0, the overall lateral error decreases. However, when $k_l = 7.0$, the lateral error exhibits strong oscillations. Consequently, a compromise value of 5.0, achieves relatively low and stable lateral errors without noticeable oscillations.

Table 4: Performance of ST Controller's Lateral Error Gains on Lateral Error

Lateral Error Gain k_l (s^{-1})	Mean / m	Max / m	Median / m
1.0	0.192	0.418	0.167
3.0	0.063	0.137	0.063
5.0	**0.008**	**0.038**	**0.008**
7.0	0.062	0.168	0.062

The lateral error metrics in Table 4, namely the mean, maximum, and median values, further confirm that the ST controller with $k_l = 5.0$ achieves the best performance across all

indicators. Based on this tuning procedure, the value of k_l is fixed to 5.0 in the subsequent simulations. Following the same trial-and-error–based tuning strategy, the remaining PP–ST controller parameters listed in Table 3 are determined analogously.

5.2. Comparison of Lateral Controllers

Subsequently, the PP, ST, and the PP-ST controller are tested and compared on the four paths described in Section 4. The first scenario considers driving forward.

As shown in Figure 5.1, all three controllers achieve close adherence to the reference circular path in terms of path tracking, as show on the left. However, the lateral error plots on the right indicate that, although the errors of the PP and ST controllers are not large and tend to stabilize after initial oscillations, they still exceed those of the PP-ST controller.

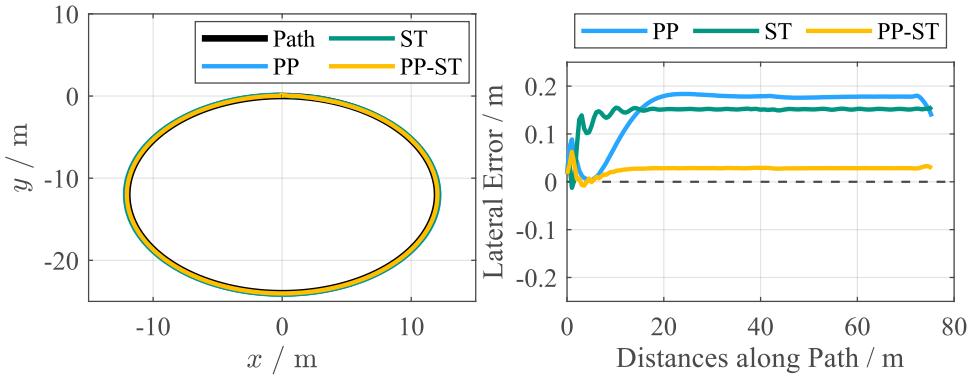

Figure 5.1. Lateral Controller Comparison during Forward Driving on a Circular Path

For the sinusoidal path in Figure 5.2, all three controllers exhibit noticeable sinusoidal oscillations in lateral error. However, the PP-ST controller shows the smallest amplitude, whereas the PP controller produces the largest. Nevertheless, the maximum absolute lateral error of all three controllers remains below 0.2 m.

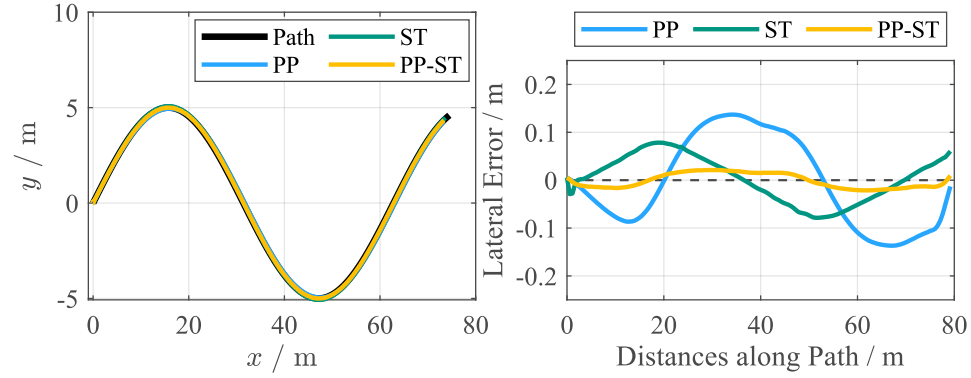

Figure 5.2. Lateral Controller Comparison during Forward Driving on a Sinusoidal Path

In the straight-line simulation shown in Figure 5.3, all three controllers exhibit strong oscillations at the beginning, with the ST controller even showing lateral swaying. However, in the later stage, all three converge to stable behavior and achieve a high degree of accuracy in straight-line tracking, with their lateral errors approaching 0 m.

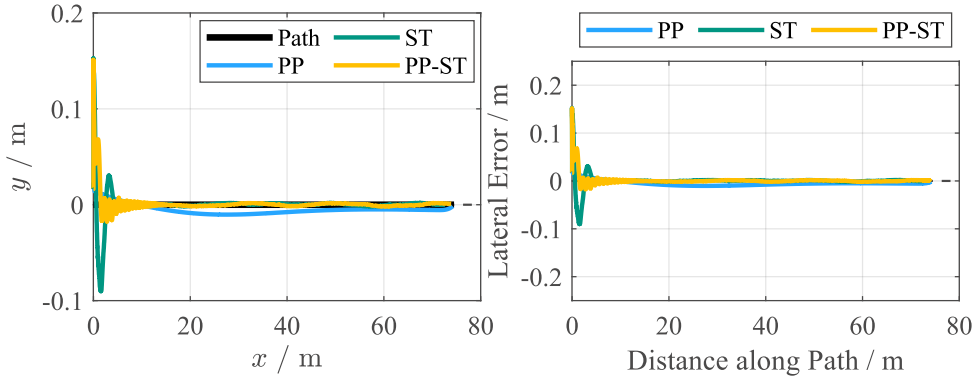

Figure 5.3. Lateral Controller Comparison during Forward Driving on a Straight Line

Figure 5.4 illustrates a real-world path. As a result, all three controllers exhibit high oscillation frequencies. Nevertheless, their overall performance remains satisfactory, with the PP-ST controller once again demonstrating the best results.

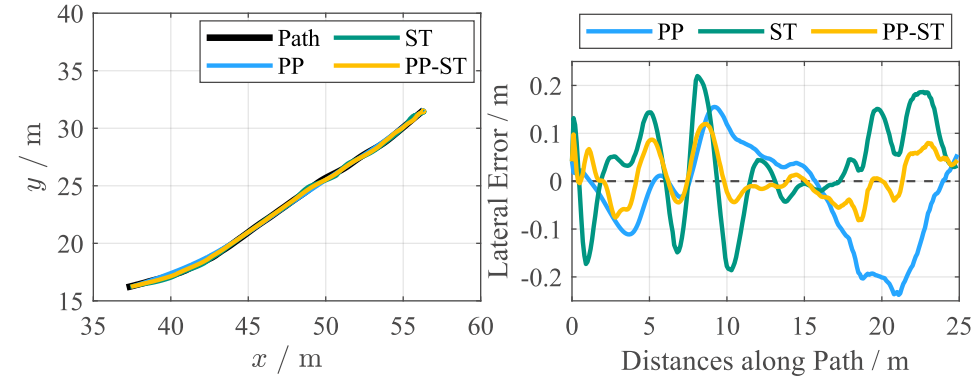

Figure 5.4. Lateral Controller Comparison during Forward Driving on a Real Path

Table 4 summarizes the controller performance in forward and backward driving across the four paths, based on identical simulation settings to ensure comparability. Although in certain cases, such as the straight-line scenario, the ST controller achieves marginally lower mean and median errors (e.g., 0.005 m and 0.001 m, respectively), the PP-ST controller introduced in this paper consistently delivers superior results in most test cases.

For forward circular and sinusoidal paths, the PP-ST controller reduces the mean error by more than 70% compared to PP and ST individually. Specifically, the mean error is 0.027 m compared to 0.153 m and 0.145 m for the circular path, and 0.014 m compared to 0.084 m and 0.042 m for the sinusoidal path. On the real path, it again halves the error (0.039 m) compared to PP and ST. This demonstrates its strong ability to track curved trajectories with high precision.

Table 4: Controller Performance on Absolute Lateral Error

Scenario Path	Lateral Controller	Mean / m	Max / m	Median / m
Driving Forward Circular Path	PP	0.153	0.184	0.178
	ST	0.145	0.157	0.152
	PP-ST	**0.027**	**0.063**	**0.028**
Driving Forward Sinusoidal Path	PP	0.084	0.137	0.087
	ST	0.042	0.078	0.041
	PP-ST	**0.014**	**0.040**	**0.015**
Driving Forward Straight Line	PP	0.007	**0.023**	0.006
	ST	**0.005**	0.153	**0.001**
	PP-ST	**0.005**	0.151	**0.001**
Driving Forward Real Path	PP	0.080	0.239	0.059
	ST	0.078	0.221	0.053
	PP-ST	**0.039**	**0.120**	**0.037**
Driving Backward Circular Path	PP	0.286	0.365	0.318
	ST	0.182	0.442	0.187
	PP-ST	**0.064**	**0.202**	**0.071**
Driving Backward Sinusoidal Path	PP	0.101	0.192	0.114
	ST	0.053	0.130	0.051
	PP-ST	**0.022**	**0.110**	**0.020**
Driving Backward Straight Line	PP	0.024	0.030	0.026
	ST	**0.004**	**0.191**	**0.001**
	PP-ST	0.005	0.201	0.003
Driving Backward Real Path	PP	0.035	0.127	**0.010**
	ST	0.028	0.127	0.013
	PP-ST	**0.021**	**0.109**	0.011

The backward driving cases further highlight the robustness of PP-ST. In the circular and sinusoidal paths, its mean error is reduced to 0.064 m and 0.022 m, respectively, significantly lower than the pure PP or ST controllers. Even in the more challenging real-path scenario, PP-ST achieves the smallest mean error (0.021 m) while maintaining stable maximum and median errors, underscoring its ability to generalize across both motion directions.

Overall, despite isolated cases where ST exhibits competitive performance, particularly in straight-line driving, the PP-ST controller demonstrates superior accuracy and stability across diverse paths and driving directions, validating its effectiveness as a more reliable solution for articulated off-highway machine lateral control.

Figure 5.5 presents boxplots of the lateral errors for all cases. The PP-ST controller achieves a maximum lateral error of less than 0.2 m, which is clearly lower than that of the other two controllers, whose performances are relatively similar to each other.

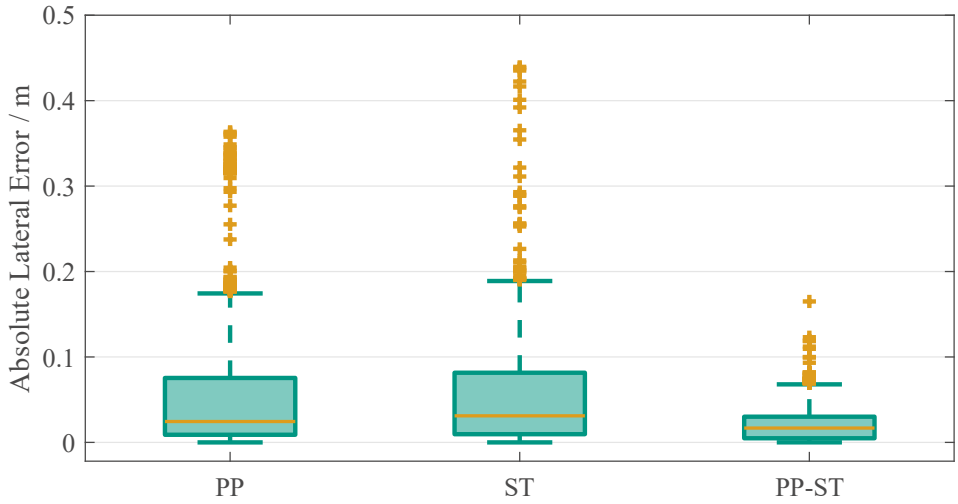

Figure 5.5. Overall Lateral Error Distributions of Absolute Lateral Controllers

5.3. Robustness Analysis of PP-ST Controller

Next, different disturbances are introduced on the sinusoidal path in Figure 5.2 to evaluate the robustness of the PP-ST controller. These disturbances include adding a noise term $2\sin(3t)$ to both the steering angle $\delta(t)$ and the velocity $v(t)$, where t denotes time; applying an additional load of 14 t to the rear vehicle of the forwarder; introducing an extra orientation offset of 45° at the initial position; and starting path tracking from a location 2 m away from the initial position.

Figure 5.6 illustrates the path-tracking performance and the corresponding signed lateral errors of the PP-ST controller under different disturbance scenarios. In the upper plot, the trajectories remain close to the reference path in most cases, with only the scenario starting with an additional orientation offset of 45° showing a visible deviation at the beginning before converging.

The lower plot shows the lateral error. When sinusoidal noise $2\sin(3t)$ is added to either the steering angle $\delta(t)$ or the velocity $v(t)$, the error exhibits oscillations but remains within 0.1 m. The additional rear-vehicle load of 14 t and the initial orientation offset of 45° cause slightly larger fluctuations than the normal case, yet the errors converge to near zero. The initial position offset of 2 m has only a minor transient effect. Overall, the controller demonstrates strong robustness under all disturbances.

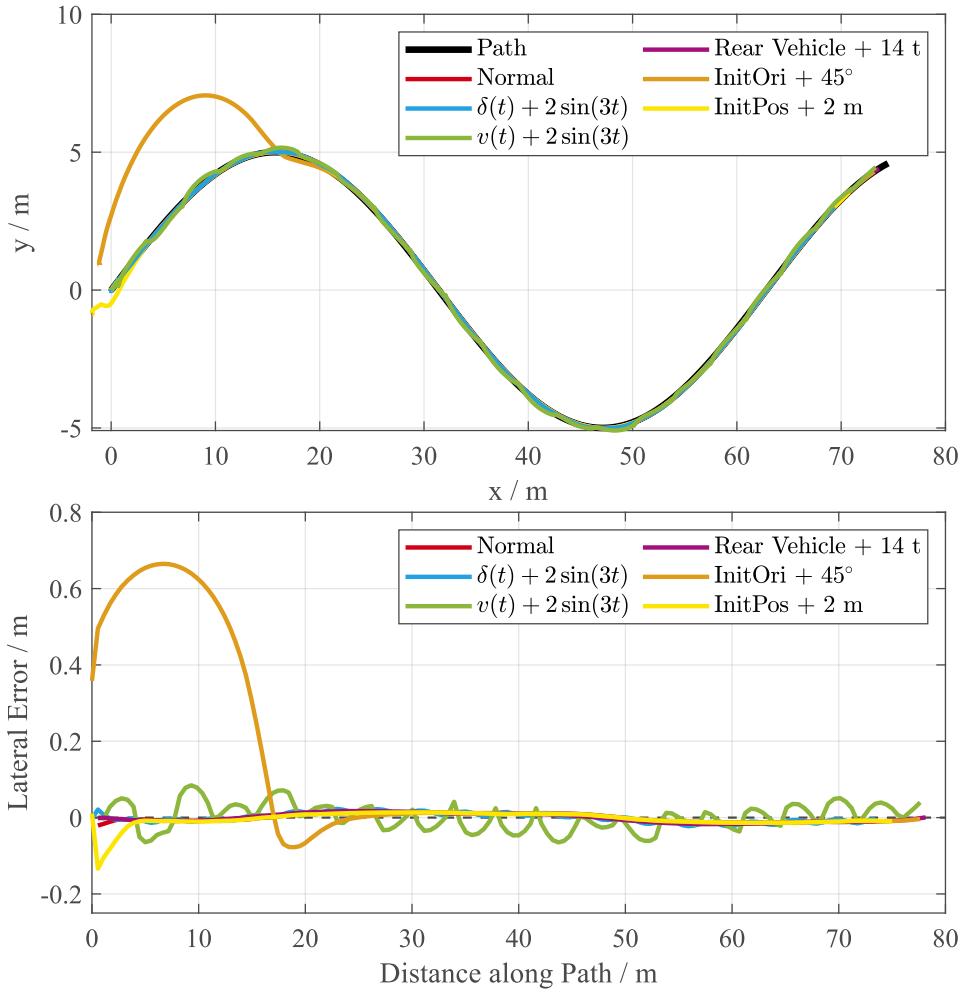

Figure 5.6. Performance of the PP-ST Controller under Different Disturbance Scenarios

The quantitative metrics in Table 5 confirm the observations in Figure 5.6. Under normal conditions (with no noise), the mean, maximum, and median lateral errors are 0.023 m, 0.049 m, and 0.024 m. Adding sinusoidal noise to the steering angle $\delta(t)$ causes only a marginal increase, with errors nearly identical to the baseline. Velocity disturbance results in higher values, with a mean of 0.068 m and a maximum error of 0.215 m. An additional rear-vehicle load of 14 t has almost no effect on the controller's performance. By contrast, the initial orientation offset of 45° produces the most significant degradation, with the maximum error rising to 3.622 m, while the mean remains relatively moderate at 0.588 m due to eventual recovery. Starting from an initial position offset of 2 m leads to a transient maximum error of 0.361 m, but the mean and median remain close to the normal case, indicating fast convergence.

Overall, both the trajectory plots and the error metrics demonstrate that the PP-ST controller is robust against most dynamic and static disturbances. Only the extreme initial orientation

offset leads to a substantial temporary degradation, while in all other cases the steady-state lateral errors remain within 0.1 m.

Table 5: Metrics of PP-ST Controller's Absolute Lateral Error under Disturbance

Scenario	Mean / m	Max / m	Median / m
Normal	0.023	0.049	0.024
$\delta(t) + 2sin(3t)$	0.024	0.054	0.024
$v(t) + 2sin(3t)$	0.068	0.215	0.060
Rear Vehicle + 14 t	0.024	0.040	0.025
InitOri + 45°	0.588	3.622	0.027
InitPos + 2 m	0.029	0.361	0.023

6. CONCLUSIONS

This paper presented a lateral control framework for Articulated Off-Highway Machines (AOHMs) by combining Pure Pursuit (PP) and Stanley (ST) controllers. The lateral error gain of the ST controller for a typical AOHM, a Forwarder, is first simulated on circular, sinusoidal, straight, and real paths demonstrated that the proposed PP–ST controller consistently outperformed standalone PP and ST controllers, achieving maximum lateral errors below 0.2 m in most cases. Robustness analysis under disturbances such as dynamic steering and velocity noise, payload variations, and initial offsets confirmed stable convergence, with steady-state lateral errors remaining within 0.1 m except for extreme orientation offsets, which caused only transient degradation. Overall, the results show that the PP–ST controller combines the complementary strengths of both methods, providing accurate, stable, and robust automated steering control for AOHMs.

7. REFERENCES

[1] M. Geimer, 'Mobile Working Machines', 2020, doi: 10.4271/9780768094329.

[2] D. Kaur, 'The impact of autonomous vehicles on mining operations: Enhancing safety and productivity through technological advancements', Scholarly Review Journal, 2024, doi: 10.70121/001c.124875.

[3] Z. Sun, 'Optimization and Evaluation of Energy Savings for Connected and Autonomous Off-Road Vehicles', 2024, doi: 10.2172/2476184.

[4] L. Gao, Y. Dong, and J. Zhao, 'Dynamic Modeling and Characteristic Analysis of Articulated Steering Vehicles', Applied Sciences, 2023, doi: 10.3390/app13085099.

[5] Z. Wang, et al., 'LiDAR-Based Tree Detection and Parameterization for SLAM in Autonomous Forestry Machinery, 2025 5th International Conference on Computer,

Control and Robotics (ICCCR), pp. 1–7, Hangzhou, China, May 16-18, 2025, doi: 10.1109/ICCCR65461.2025.11072654.

[6] X. Li, et al., 'A Modelling Method for All-Axle Steered Multi-Articulated Vehicles', 2024 UKACC 14th International Conference on Control (CONTROL), pp. 236–241, Winchester, United Kingdom, 2024, doi: 10.1109/CONTROL60310.2024.10532122.

[7] A. Ajorkar and Y. He, 'Design of autonomous driving controls for multi-trailer articulated heavy vehicles', Journal of Vibration and Control, 2025, doi: 10.1177/10775463251313657.

[8] L. Michiels, C. Geiger, and M. Geimer, 'Autonomous Driving on Skid Tracks for Forestry Machines', 2025, doi: 10.5445/IR/1000179648.

[9] D. Jeong and S. B. Choi, 'Tube-Based Robust Model Predictive Control for Tracking Control of Autonomous Articulated Vehicles', IEEE Trans. Intell. Veh., 2024, doi: 10.1109/TIV.2023.3320795.

[10] N. Sun, W. Zhang, and J. Yang, 'Integrated Path Tracking Controller of Underground Articulated Vehicle Based on Nonlinear Model Predictive Control', Applied Sciences, 2023, doi: 10.3390/app13095340.

[11] L. Liu, et al., 'Path Tracking Control for Underground Articulated Vehicles with Multi-Timescale Predictive Modeling', Actuators, 2025, doi: 10.3390/act14100477.

[12] F. M. Barbosa, et al., 'Robust path-following control for articulated heavy-duty vehicles', Control Engineering Practice, 2019, doi: 10.1016/j.conengprac.2019.01.017.

[13] P. I. Corke and P. Ridley, 'Steering kinematics for a center-articulated mobile robot', IEEE Trans. Robot. Automat., 2001, doi: 10.1109/70.928568.

[14] R. C. Conlter, 'Implementation of the Pure Pursuit Path Tracking Algorithm', Robot. Inst., Tech. Rep. CMU-RI-TR-92-01, Pittsburgh, PA, USA, 1992.

[15] J. M. Snider, 'Automatic Steering Methods for Autonomous Automobile Path Tracking', Robot. Inst., Tech. Rep. CMU-RI-TR-09-08, Pittsburgh, PA, USA, 2009.

[16] J. Morales, et al., 'Pure-Pursuit Reactive Path Tracking for Nonholonomic Mobile Robots with a 2D Laser Scanner', EURASIP J. Adv. Signal Process., 2009, doi: 10.1155/2009/935237.

[17] A. E. Bousskoul, I. Ouachtouk, and A. Ait Elmahjoub, 'Control strategies for autonomous vehicle path tracking: A comparative study of PID, Pure-Pursuit, and Stanley methods', EPJ Web Conf., 2025, doi: 10.1051/epjconf/202533006001.

[18] G. M. Hoffmann, et al., 'Autonomous Automobile Trajectory Tracking for Off-Road Driving: Controller Design, Experimental Validation and Racing', 2007 American Control Conference, pp. 2296–2301, New York, NY, USA, 2007, doi: 10.1109/ACC.2007.4282788.

[19] Y. Cao, et al., 'PP-ST: An Indoor Mobile Robot Path Tracking Algorithm', IEEE Access, 2023, doi: 10.1109/ACCESS.2023.3326247.

Biographies

Zezhou Wang received his B. Sc. in Mechanical Engineering in 2022 and his M. Sc. in Automotive Engineering in 2024, both from RWTH Aachen University, Germany. He is currently working as a Research Associate at the Institute of Mobile Machines (Mobima) at the Karlsruhe Institute of Technology (KIT). His research focuses on localization, intelligent control and Sim2Real technologies of highly automated and autonomous forestry machines.

Magdalena Janocha received her B. Sc. in Mechatronics and Information Technology in 2025 and is currently pursuing her M. Sc. in Mechatronics and Information Technology at the Karlsruhe Institute of Technology (KIT), Germany. Her research interests include intelligent control of articulated vehicles.

Lukas Michiels received his B. Sc. in Mechanical Engineering in 2017 and his M. Sc. in Mechanical Engineering in 2019, both from the Karlsruhe Institute of Technology (KIT), Germany. In 2024, he obtained his Dr.-Ing. (Ph.D.) degree from KIT. His doctoral research focused on the development of driving functions and environment perception using artificial intelligence for the (semi-)autonomous operation of forestry machines, as well as the simulation of coupled fluid–structure interaction in the drive systems of mobile working machines.

Benjamin Kazenwadel received his B. Sc. in Mechanical Engineering in 2019 and his M. Sc. in Mechanical Engineering in 2021, both from the Karlsruhe Institute of Technology (KIT), Germany. He also earned the title Magister en Energia y Ambiente (Master in Energy and Environment) from the Instituto Tecnológico de Buenos Aires (ITBA), Argentina. He is currently working as a Research Associate at the Institute of Mobile Machines (Mobima) at KIT. His research focuses on the development of assistance systems to improve the efficiency of agricultural machinery.

Marcus Geimer received the Diploma degree in mechanical engineering from the RWTH Aachen University, Germany, in 1990, and the Ph.D. degree from the Institute of Hydraulics and Pneumatics, today named the Institute for Fluid Power Drives and Systems, RWTH Aachen University. Since 2005, he has been a Full Professor and the Director of the Institute of Mobile Machines (Mobima), Karlsruhe Institute of Technology (KIT), Germany. He started his industrial career in 1995 in the field of construction at the company Krupp Berco Bautechnik GmbH, Germany, where he was the Leader of the research group for hydraulic breakers. In 2000, he was with Bucher Hydraulics GmbH, Germany, where he led the construction and customer development for mobile hydraulics.